Spatial Arrangement of a Counter-Rotating Dual Rotor Wind Turbine

Csaba Hetyei, Ildiko Molnar and Ferenc Szlivka

May 9, 2023

Spatial Arrangement of a Counter-Rotating Dual Rotor Wind Turbine

Csaba Hetyei[a], Ildikó Molnár[b], Ferenc Szlivka[b]

[a]Óbuda University, Doctoral School on Safety and Security Sciences, Budapest, Hungary

[b]Óbuda University, Donát Bánki Faculty of Mechanical and Safety Engineering, Budapest, Hungary

Abstract

Nowadays increasing energy demand and the current energy crisis in Europe highlighted the need for independent and cheap energy sources which can be produced at the place of use. A good example of this energy sources are the renewables, from which wind energy is one. Humanity is using wind energy since the beginning of the history but electrical energy generation from the wind started at the end of the 19th century. During the evolution of wind energy utilization, wind turbines are becoming more and more efficient. A special kind of these turbines are the non-conventional wind turbines which are aiming to be efficient in a special condition. One of these new turbine designs is the CO-DRWT (Counter-Rotating Dual Rotor Wind Turbine), where there are two rotors in one tower.

During our research, we examined some layouts for a CO-DRWT. In these spatial arrangements, we were able to change the second rotor's axial and radial positions. Within two in axial and one diameter in the radial region, we were running CFD (Computational Fluid Dynamics) simulation to determine the interaction of the two turbines and for calculating the overall power coefficient (c_p) for the two rotors. Meanwhile, in our analysis, we defined some spatial arrangements where the CO-DRWT's overall c_p is less than the c_p of a Single Rotor Wind Turbine (SRWT) from the same geometry. We also defined regions where the CO-DRWT's c_p is higher than the SRWT's. With our geometry and with our simulation's boundary conditions we find the optimal place for operating a CO-DRWT is the R = 0D radial distance with A = 2.1D axial distance (where the D is the rotor's diameter) where the c_p is 0.514, also the worst arrangement is the R = 0.35D with A = 1.25D where the c_p = 0.354, while an SRWT's c_p from the same geometry is 0.377. According to our simulations, the energy density and the power coefficient of an optimized CO-DRWT are 1.363 times higher than an SRWT has.

Keywords

CFD, CO-DRWT, Design of Experiments, DOE, Dual Rotor Wind Turbine, Optimisation

1. Introduction

The utilization of wind energy has a long history. It started with the sailing and the wind-powered organ of the Hero of Alexandrina. The first known windmill was built in Nastifan in the 9th century for grinding. In Europe, windmills started to spread in the 12th century. Until the 19th century, windmills were used for grinding or lifting water [1]. In 1887, James Blyth built the first Vertical Axis Wind Turbine (VAWT) to generate energy in his rear garden in Marykirk for energy generation. In 1888, Charles Brush built the first Horizontal Axis Wind Turbine (HAWT) to generate energy in Cleveland [3]. Charles Brush's wind turbine has "only" 12 kW capacity [3], while nowadays typical turbine capacities are in the MW scale, thanks to research and developments.

An indicator of wind energy utilisation is the total installed turbine capacity, which was 24 GW in 2001, 238 GW in 2011, 488 GW in 2016, and 837 GW in 2021. The mostly installed turbine capacity is onshore but offshore installation is also possible. Currently, the total installed turbine's capacity is 780 GW onshore and 57 GW offshore [5].

Generally, and during energy crises [6], researchers and energy providers try to find solutions to meet the energy demand. To solve the necessary electricity supply for users, wind turbine developers optimise their turbines for different environments [7], e.g., there are diffusers to catch more wind or to increase the wind's kinetic energy [8][9], or there are airfoil [10] and blade designs [11] for specific environments, or there are new places where the wind turbines can produce electricity like a solar chimney [12] or like a turbine installed on buildings in cities [13].

Besides the core turbine design and optimisation, new kinds of wind turbines also appear in the energy generation marketplace, which are unconventional wind turbines. These types of new wind turbines are modified in some respects. Two examples in this category are the Dual Rotor Wind Turbines [14][15] which are multiple rotor turbines made from traditional and the second is the modified rotors e.g., the Archimedes Screw Turbine [16], which are highly modified turbines for special environments and their needs.

Next to the research and development of wind turbines, there were also developments in turbine-related industries and products, such as operation, performance, and diagnostic monitoring [17] [18]. The previous examples mainly focused on the horizontal axis wind turbines, but there are energy-generating systems containing more renewable and non-renewable sources, which can be installed in the urban and the non-urban zones. In our energy needy system, the smallest energy-consuming unit can be a single house [19] which can produce energy with solar, geothermal or heat pumps [20] for families.

2. Different impeller layouts for higher extractable power

In our research, we analysed a Counter-Rotating Dual Rotor Wind Turbine (CO-DRWT), which is an unconventional wind turbine. We chose this wind turbine type because it has a bigger performance than a single or a Co-Rotating Dual Rotor Wind Turbine [14] [22]. We used a CO-DRWT for our simulations, which we used in our previous studies. Firstly, we created a wind turbine geometry which we mirrored. The original part is our first rotor and the second is the mirrored one. These rotors are rotate in opposite directions, therefore if the radial gap is 0.5 in diameter (100 mm) or more, the second blade is not covered by the first. This turbine is shown in the following figure.

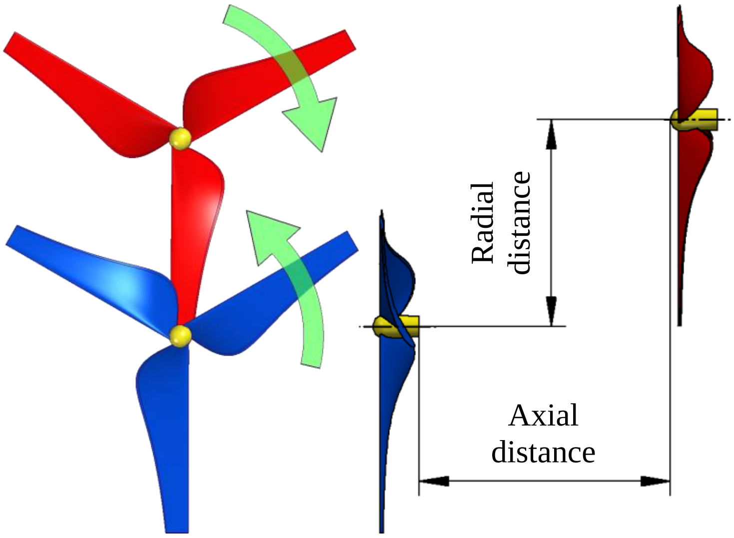

1. Figure. CO-DRWT with the indication of the rotors' rotating direction and the variable axial and radial distances

In the 1st figure, the rotational directions are shown with green arrows. For our research, we were able to change the axial and radial distances between the CO-DRWT's rotors, these distances are indicated. The distances were de-dimensioned with the rotor's diameter, which was 200 mm, therefore the R=1D distance is 1·200 mm=200 mm in the radial direction. The minimal distance was 0.005D and the maximum was 2D for the axial distance and 0D was the minimal and 1D for the radial distance.
To measure the wind turbines efficiency, we used the power coefficient (c_p) for our CO-DRWT during our tests which can be calculated from the torque on the blades and from the incoming flow with the following equation:

$$c_p = \frac{P_{turbines}}{P_{wind}} = \frac{T_1 \cdot \omega_1 + T_2 \cdot \omega_2}{\frac{1}{2} \cdot \rho \cdot A \cdot v^3} = \frac{P_{turbine\ 1} + P_{turbine\ 2}}{P_{wind}} = \frac{P_{turbine\ 1}}{P_{wind}} + \frac{P_{turbine\ 2}}{P_{wind}} = c_{p1} + c_{p2} \tag{1}$$

In the previous equation c_p is the CO-DRWT overall power coefficient, c_{p1} and c_{p2} are the power coefficient of the first and the second turbine, $P_{turbines}$ is the CO-DRWT overall performance, $P_{turbine1}$ and $P_{turbine2}$ are the first and the second turbine's performance and P_{wind} is the wind performance. T_1 and T_2 are the torque on the first and on the second turbine, ω_1 and ω_2 are the angular velocity of the first and the second turbine. ρ, is the density of the air, A is the swept area of the wind turbine's blade and v is the wind's velocity in the freestream area.
The swept area in the previous equation depends on the radial shift of the two turbines, and its value is between $d^2 \cdot \pi/4$ and $2 \cdot d^2 \cdot \pi/4$, where d is the diameter of the turbine. This area is shown in the next figure.

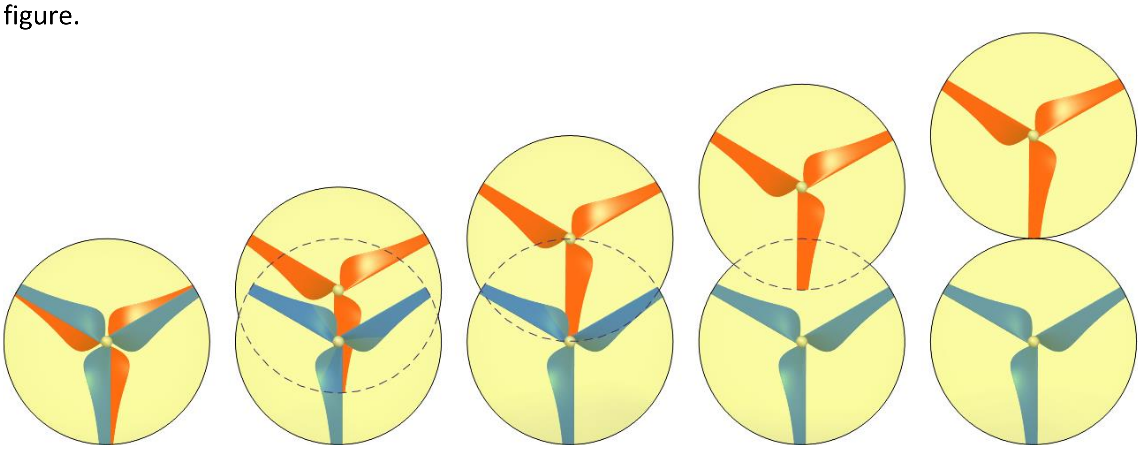

2. Figure. Swept area for different CO-DRWT layouts (from 0 to 1 diameter radial shift)

In our previous research, we measured the torque on the turbines then we calculated the power coefficient [23]. After the physical testing, we started to use CFD software to simulate the different axial distances [24]. For our simulation, we used Reynolds Averaged Navies Stokes (RANS) equations-based CFD software. This numerical simulation method is based on the continuity, momentum, and energy equations which were solved iteratively with the SIMPLE algorithm.

A single rotor's maximum power coefficient (c_p) by the Betz law is c_p=16/27≈59.259%. The Betz law is a theoretical limit for a wind turbine with an ideal flow and boundary conditions, where the turbine has an infinite number of blades. The Betz law was created at the beginning of the 20th century. 8 decades after Betz, Gorban *et al.* created their model, known as the GGS model. By the GGS model, a wind turbine's maximum power coefficient (c_p) is c_p=30.113 % [25]. Using CFD simulations and measurement, the wind turbines' c_p is between these two values provided by the Betz law and the GGS model.

3. Simulation Parameters

For our simulations [24] we used Simcenter FLOEFD with the same boundary conditions as we used for the measurements [23]. The wind velocity in the freestream region (v_∞) was 3.79 m/s, the ambient pressure was 1 atm, the fluid was "air" from the CFD software's database, and the temperature was 20 C. The tip speed ratio (λ), which is the ratio of the wind turbine's angular velocity and the free stream velocity, was 4. The tip speed ratio can be calculated with the following equation:

$$\lambda = \frac{\omega \cdot R}{v_\infty} \tag{2}$$

In the previous equation, the λ is the tip speed ratio, ω is the angular velocity, R is the radius of the blade, and v_∞ is the freestream velocity.
For the simulations, we used a rectangular domain, within which we used Cartesian mesh with polyhedral elements on the surfaces of the wind turbines. The mesh contains 2.8–3 million elements depending on the CO-DRWT's position.

The k-ε turbulence model was used for the turbulence modelling. For validation, we ran simulations in steady and unsteady states, but for the optimization of the spatial arrangement, we used only the steady-state results. In the steady-state, to model the turbine's rotation we used the Mixing Plane method.
During our simulations, we monitored the torque and the static pressure on the turbines' blades, and the averaged and maximum velocity, static, and total pressure in the whole computational domain and in the rotating regions. We used these parameters as finishing conditions. If all the parameters converged and the simulation ran for at least 10,000 iterations, the calculation ended.

4. CFD Results

After running our simulations, in the turbines' region, we had a similar flow field. Near the wind turbines' region in the wake region, the velocity was generally lower than in the freestream region. The first turbine slowed down the incoming air by taking out the air's kinetic energy to the rotational motion. The flow which reached the second turbine was turbulent and slower than the wind which arrived at the first turbine. Depending on the configuration the wake region's shape changed. Typical velocity distribution of the CO-DRWT is shown in the next figure.

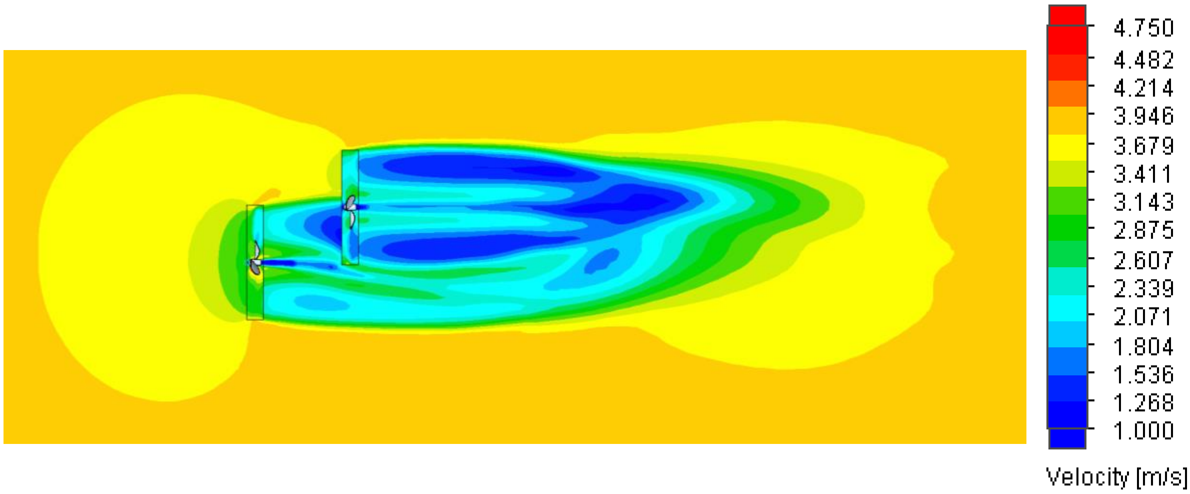

3. Figure. Flow field in the turbines' region (velocity distribution, steady state, A = 0.5D, R = 0.75D axial and radial distance)

Using the (1) equation we were able to calculate the power coefficient for each rotor (c_{p1} and c_{p2}) and the overall power coefficient (c_p) of the CO-DRWT. In the following figures the c_{p1}, c_{p2}, and c_p are shown for the CO-DRWT different axial and radial shifts.

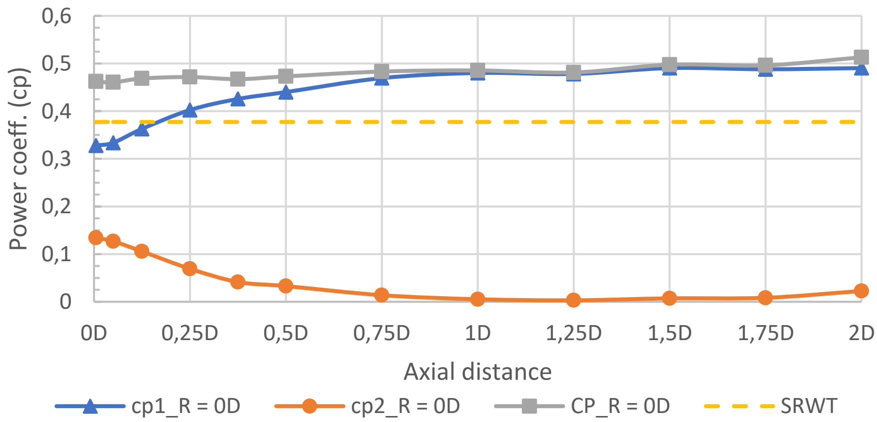

4. Figure. Power coefficient for the first (c_{p1}), second (c_{p2}) rotors and the overall c_p for the CO-DRWT with R = 0D radial distance (0 mm)

In the previous figure (4. Figure), the CO-DRWT's radial shift was 0D, therefore the rotors were coaxial. The axial gaps were between 0.005D and 2D. The power coefficient of the first turbine increased, while the power coefficient of the second rotor (c_{p2}) decreased with the axial distance. The yellow dashed line is the power coefficient of a single rotor turbine (SRWT), which was simulated with the same geometry. The power coefficient of the second rotor (c_{p2}) was in each case lower than the power coefficient of the SRWT (c_{p_SRWT}), while the power coefficient (c_{p1}) of the first rotor was higher than the c_p of the SWRT after A≈0.15D axial distance. The overall c_p of the CO-DRWT was higher than the SRWT's in each configuration.

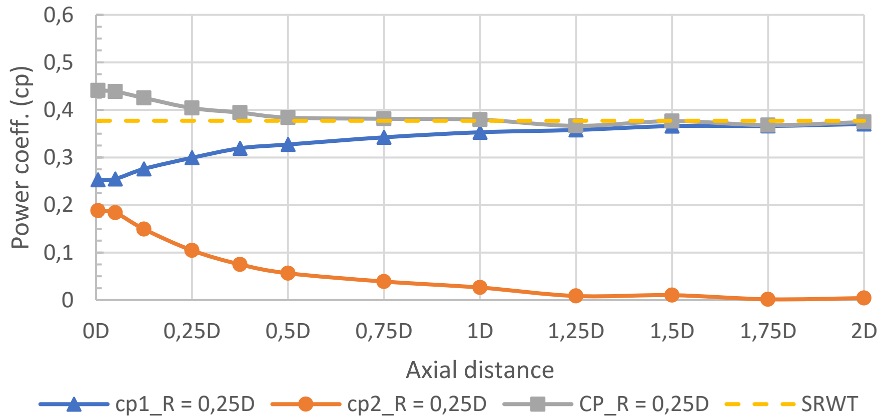

5. Figure. Power coefficient for the first (c_{p1}), second (c_{p2}) rotors and the overall c_p for the CO-DRWT with R = 0.25D radial distance (50 mm)

In the previous figure (5. Figure) the radial distance was R=0.25D (50 mm). In this case, the c_{p1} increased and the c_{p2} decreased with the growth of the axial distance, like in the case of R=0D case. The overall c_p of the CO-DRWT was higher than the power coefficient of the SRWT (c_{p_SRWT}), with a relatively small axial gap. While the axial distance rise, the c_p of the CO-DRWT decreased. Near A=1.25D axial distance, the power coefficient of the CO-DRWT decreased lower than the c_p. of the SRWT. Between the A=0.75D and the A=2D axial distances, the power coefficient of the CO-DRWT was similar to the SRWT.
Comparing this case to the R=0D, the c_{p1} was lower in each axial distance than in the R=0D and the c_{p2} too.

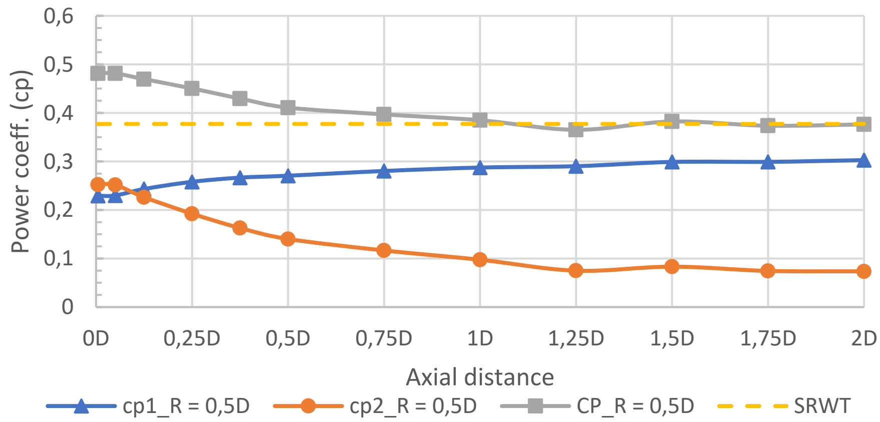

6. Figure. Power coefficient for the first (c_{p1}), second (c_{p2}) rotors and the overall c_p for the CO-DRWT with R = 0.5D radial distance (100 mm)

In the previous figure (6. Figure) the c_{p1} increased with the axial distance like in the R=0D and R=0.25D cases but the difference between the rise between the starting and the end distance was smaller. The slope of the c_{p2}, compared to the previous cases (R=0D, R=0.25D) was also smaller. In comparison with the two previous cases, the starting values of the c_{p1} was lower and the c_{p2} was higher.
The overall c_p for the CO-DRWT was similar to the R=0.25D but its values were different. It started with a high value which decreased with the growth of the axial distance. In the region R=1D and R=2D, the CO-DRWT's overall power coefficient was similar to the SRWT's c_p.

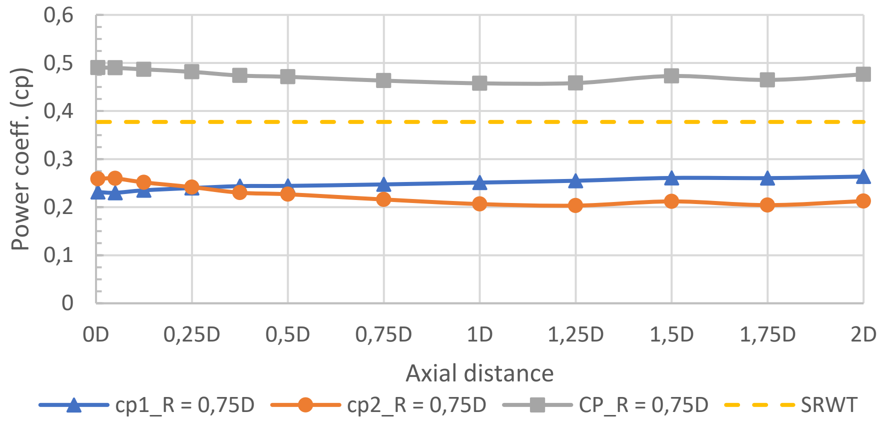

7. Figure. Power coefficient for the first (c_{p1}), second (c_{p2}) rotors and the overall c_p for the CO-DRWT with R = 0.75D radial distance (150 mm)

In the previous figure (7. Figure), where the CO-DRWT has R=0.75 radial distance, the c_{p1} and the c_{p2} show a rise and a fall, but the differences between the two ends are smaller than they were in the R=0D, R=0.25D, and R=0.5D cases. The c_{p1} and the c_{p2} values are similar. They are close to each other.

The overall c_p of the CO-DRWT for each configuration is higher than the power coefficient of the SRWT (c_{p_SRWT}). The curve of the c_p of the CO-DRWT also decreased.

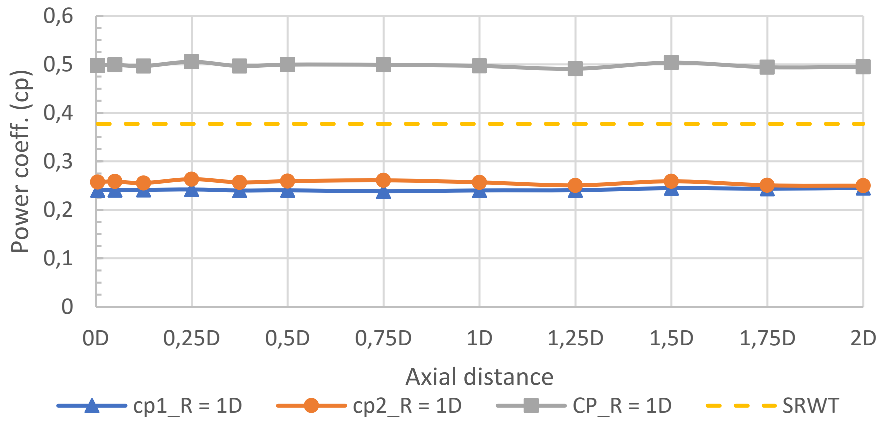

8. Figure. Power coefficient for the first (c_{p1}), second (c_{p2}) rotors and the overall c_p for the CO-DRWT with R = 1D radial distance (200 mm)

In the previous figure (8. Figure) the radial distance was 1 diameter. In this case, the swept area of the first rotor does not cover the second rotor and its swept area. The power coefficient of the two rotors was similar and with the growth of the axial distance, they do not change much. In this case, the two rotors have some effects on each other, because the power coefficients were not the same as the c_p of the SRWT (c_{p_SRWT}). The overall c_p of the CO-DRWT was higher in each case than the SRWT's.

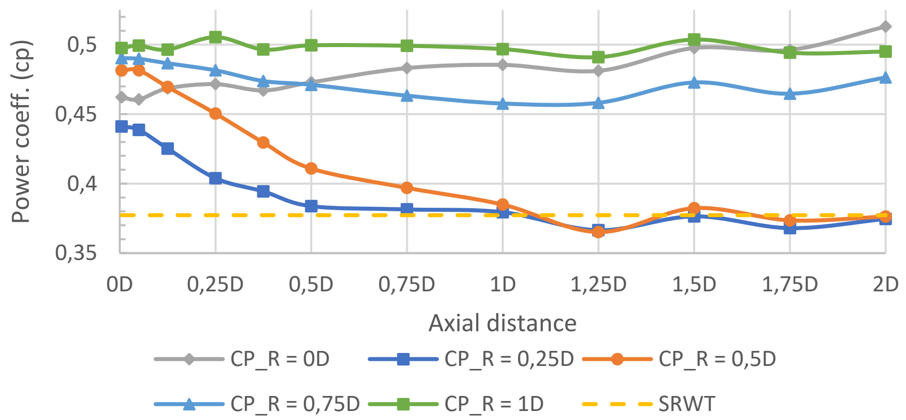

9. Figure. Overall power coefficients for the different CO-DRWT configurations

In the previous figure (9. Figure) the overall c_p of the CO-DRWT are summarized and compared with the c_p of the SRWT (c_{p_SRWT}). We can observe the power coefficients,

- in the R=0D case (when the two rotors have the same axis) the overall c_p shows a rise. We assume that the reason for this increase in the c_p is because of the influence of the second rotor on the first rotor. This can be seen in Fig. 4, where the c_{p1} increased more than the power coefficient of the SRWT, while the c_{p2} decreased (almost to zero).
- in the R=0.25D and in the R=0.5D we can see a similar slope for the power coefficients. The c_p starting values are higher than they decreased and in some cases, its values are lower than the SRWT's.
- in the R=0.75D we can see a slope in the first half of the examined axial distance, then after the A=1D axial distance, the overall c_p rose.
- in the R=1D case (when the two rotors' swept areas do not cover each other), the overall c_p was almost the same for each axial distance. We assume the reason for this was the flow which reached the second turbine. This flow (in the second turbine's region) was not turbulent and did not disturb as in the R=0.25D, R=0.5D and the R=0.75D cases.

5. Surface fittings on the CFD's results

Using our CFD results shown in Figure 9 [24], we created surfaces for layout optimisation. In the next figures, we used a CAD system (Solid Edge) with a self-made coordinate system for easier representation. In the next figure (Fig. 10) a surface is shown with a cubic interpolation, based on the CFD results.

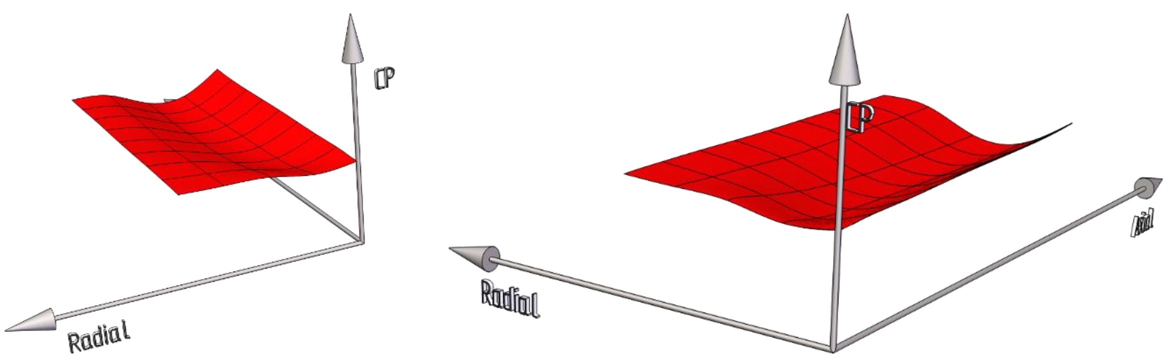

10. Figure. The fitted surface of the overall power coefficients for the different CO-DRWT configurations

The surface from Figure 10. was not appropriate for optimisation because the highest c_p was the highest simulated c_p at the R=0D and A=2D position. For the previous reason, we increased our surface for the optimisation process with the following considerations:

- In the negative direction of the "Axial" axis, we mirrored the power coefficients with negative values (thereby the plane for the mirror was the Axial-Radial plane).
- In the positive direction of the "Axial" axis, we copied the power coefficients' values until the A=2.5D distance without changing its values.
- In the negative direction of the "Radial" axis, we mirrored the power coefficients without changing their values (thereby the plane for the mirror was the c_p-Axial plane).
- In the positive direction of the "Radial" axis, we copied the power coefficients' values until R=1.5D distance without changing their values.

The surface created with our assumption is shown in the following figure.

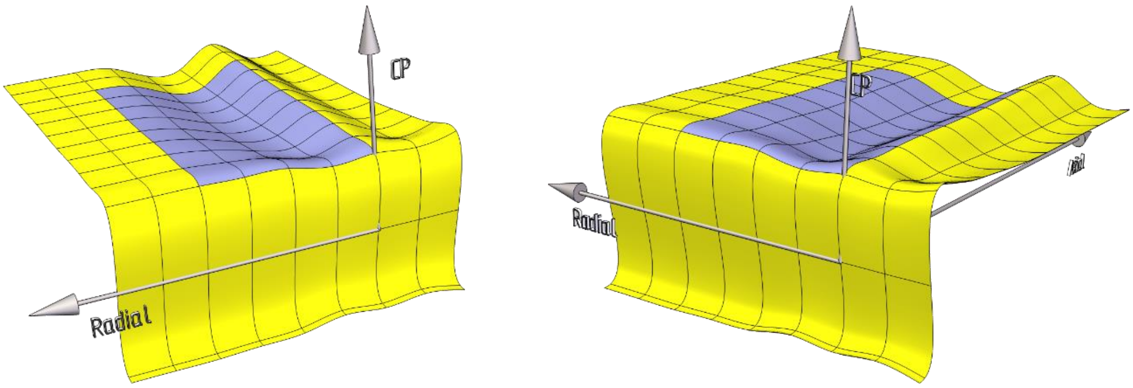

11. Figure. CO-DRWT's power coefficient in the region augmented by assumptions

In the previous figure, the original zone of our simulation is coloured in purple, meanwhile, the region of the assumption is yellow. The original surface from Figure 10 and the enlarged surface from the Figure 11 are different due to the different boundaries. The differences are shown in Figure 12.

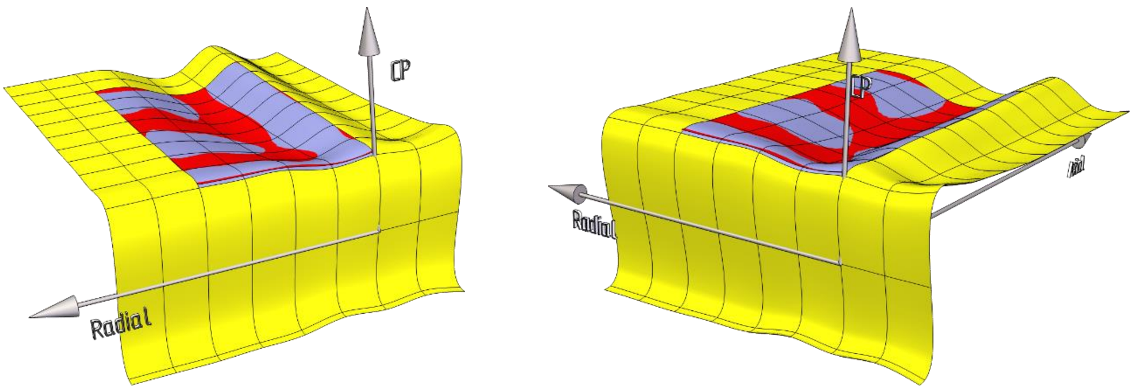

12. Figure. Original vs. augmented surface

In the previous figure, we could observe that the red (original) surface was higher in some regions than the purple one (augmented surface with the assumptions). In those regions where the purple surface covers the red, the augmented surface has higher c_p-s due to the surface fitting methodology.

For comparison, we created a surface for a Single Rotor Wind Turbine too. As it was expected (based on the results from Fig. 4 to Fig. 9), in some regions, this surface is higher than the surface which is increased by our assumption. In the next figure, the SRWT's surface is coloured green while the surface with the augmented values has the same colour as before.

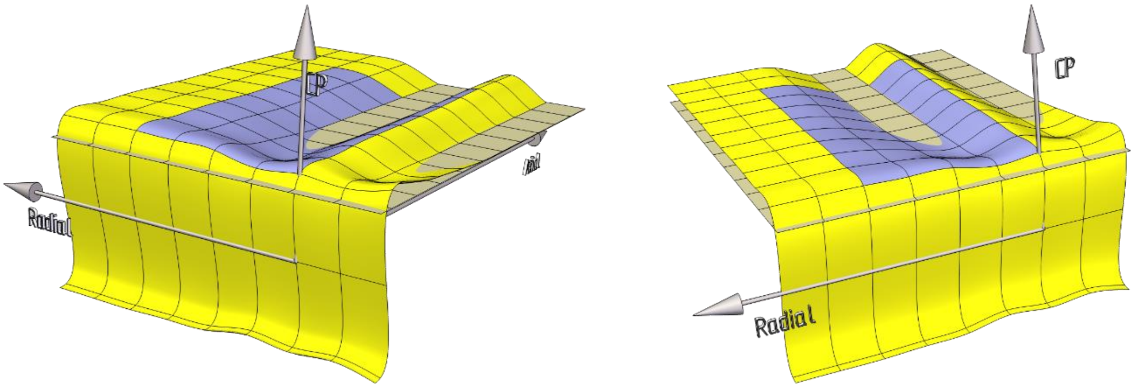

13. Figure. Augmented surface vs. a SRWT's c_p

For the optimisation process, we only used the overall power coefficient of the CO-DRWT (c_p), therefore the c_{p1} and c_{p2} values were ignored.

For our optimisation process, we created an optimisation script in MATLABA 2022a, where we used the cubicinterp, poly33 and poly55 methods. Using these surface fitting methods, the highest power coefficients and their positions are shown in the following table.

Table 1. Highest power coefficients with their positions

Interpolation type	Highest power coefficient (c_p)	Radial distance for the highest c_p	Axial distance for the highest c_p
poly33	0.634	1.5D	0.9D
poly55	0.649	1.4D	0.35D
cubicinterp	0.514	0D	2.1D

The poly33 and poly55 methods create polynomial surfaces which are based on the input c_p-s but the surfaces do not lie on the entered points. While the cubicinterp method creates a surface with cubic spline interpolation, where the surface fits with the input data. From the previous interpolations, the surface lies on the input data only with the cubicinterp method, which we chose for our optimisation.

The surfaces with are created with poly33 and poly55 algorithms are shown in the following figure.

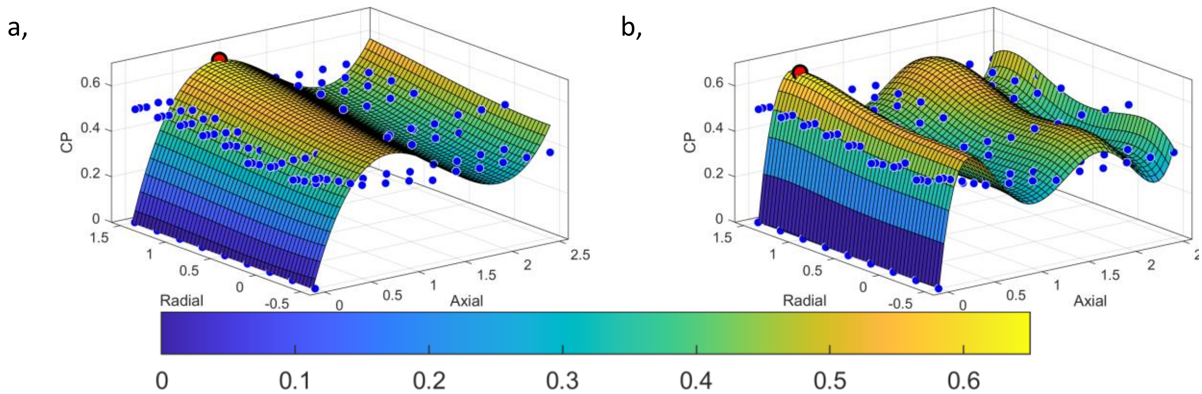

14. Figure. CO-DRWT's maximum power coefficient on a surface which was created by polynomial interpolation. a, surface with poly33; b, surface with poly55

The surface which is created with a cubic spline interpolation is shown in the following figures (Fig. 15 and Fig. 16). The surface is coloured by its c_p value, the maximum value is marked with a black-edged red dot, while the input data points are represented with a blue dot.

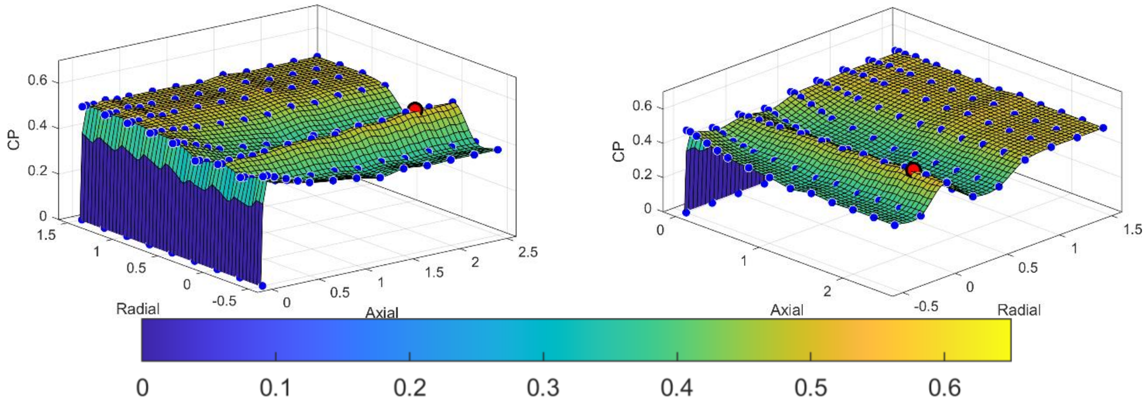

15. Figure. CO-DRWT's maximum power coefficient on a surface which was created with a cubic spline interpolation

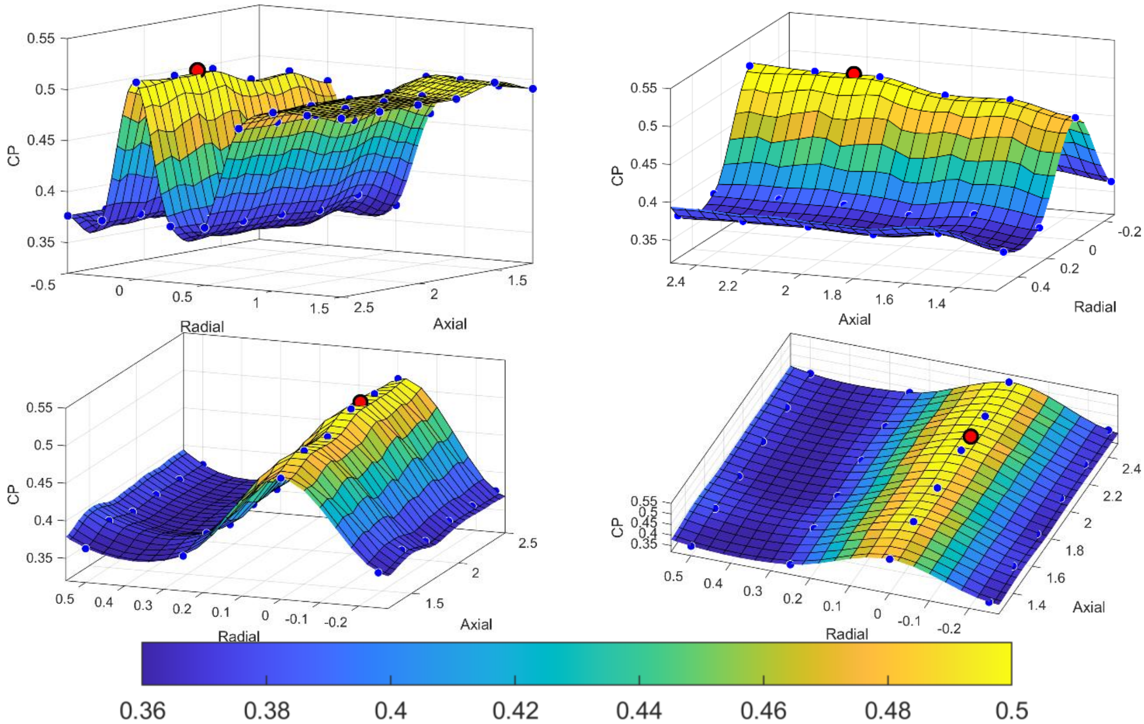

16. Figure. CO-DRWT's maximum power coefficient and its region

As in the previous figures (Fig. 4-9. and Fig. 13), the c_p is lower in some regions than the SRWT's power coefficient (c_{p_SRWT}). We changed our script to determine the worst-case layout. The minimum search algorithm looked for the minimum value in the region of the original simulations (from A=0.005D to A=2D and from R=0D to R=1D). We used this limitation because when we enlarge our surfaces in the negative Axial direction, we mirrored our results with a negative value, therefore this region had the lowest overall power coefficients on the surface.

The lowest overall power coefficient of the CO-DRWT in the region of the simulations was c_p=0.354 at the R=0.35D radial with A =1.25D axial distance. In the following figures, (Fig. 17 and Fig 18) the minimum value is marked on the surface with a black dot with a red border.

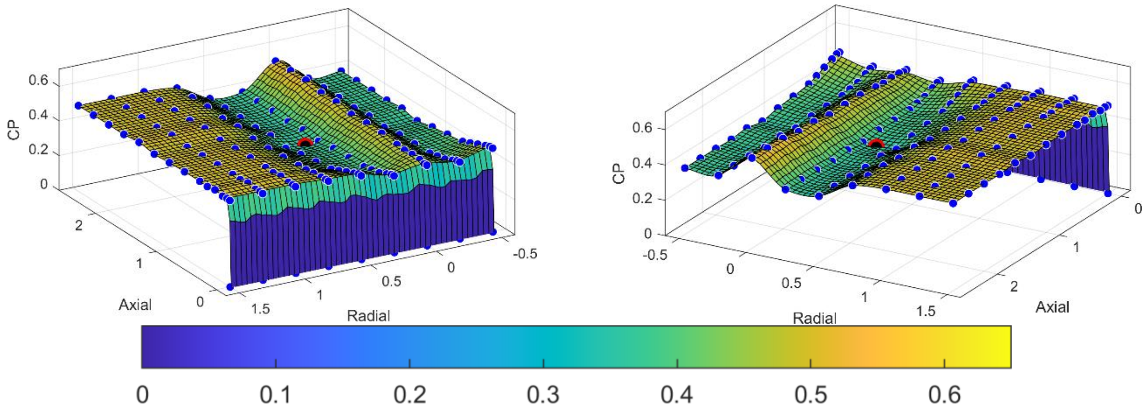

17. Figure. CO-DRWT's minimum power coefficient on a surface which was created with a cubic spline interpolation

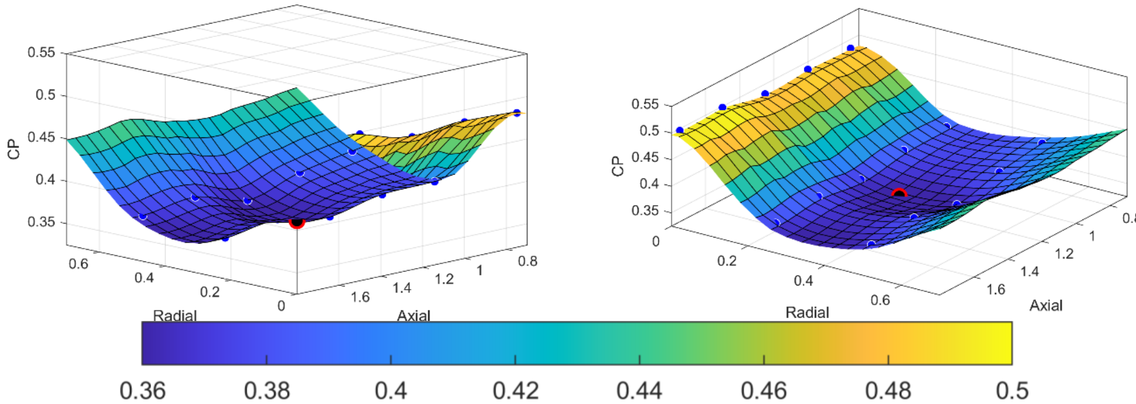

18. Figure. CO-DRWT's minimum power coefficient and its region

The minimum and the maximum values are shown on the surface with their previous marks (the maximum is a red dot with a black corner, and the minimum is a black dot with a red border).

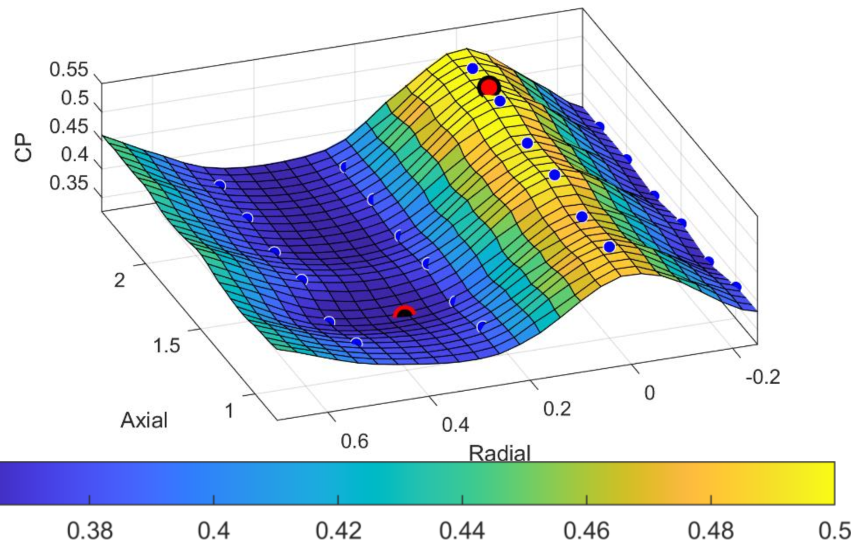

19. Figure. CO-DRWT's maximum and minimum power coefficient and their region

To find the regions which are more efficient than the SRWT, we recoloured the previous figure with the limit of the power coefficient of the SRWT's (c_{p_SRWT}=0.37727) and then subtracted the regions which are lower than the SRWT's c_p. The regions which have a higher power coefficient than an SRWT are shown in the following figures.

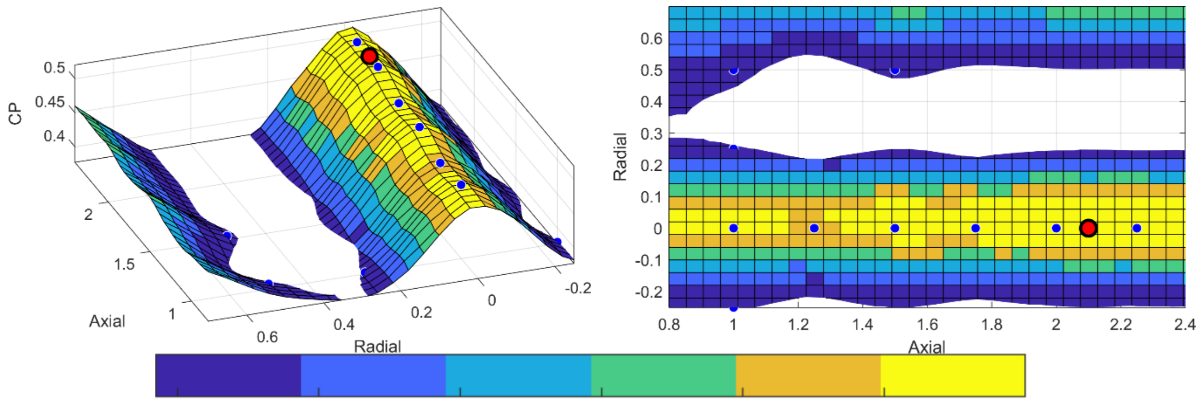

20. Figure. Power coefficients and their regions which are higher than an SRWT's c_p (near the surface's maximum)

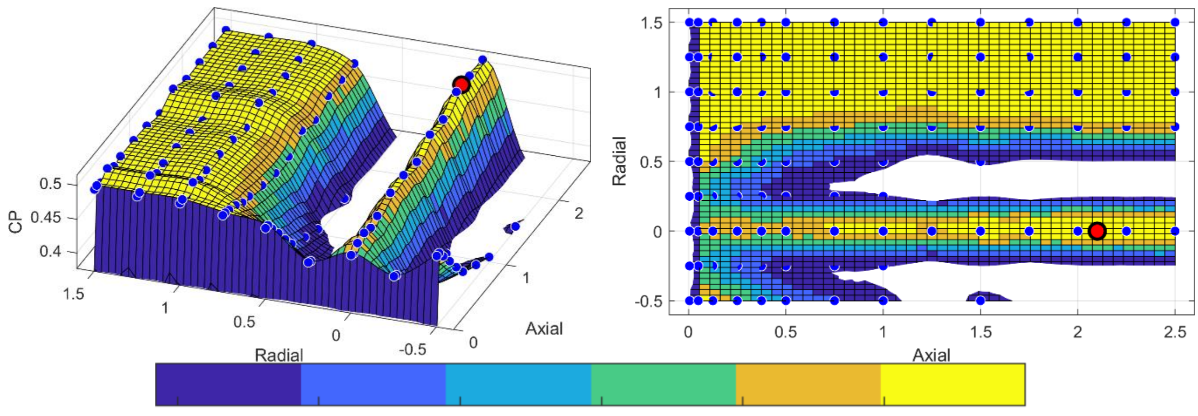

21. Figure. Power coefficients and their regions which are higher than an SRWT's c_p

If we limit the radial and axial axes to the simulation's original region (A=0.005D to A=2D and R=0D to R=2D) we have the power coefficient distribution which is shown in the following figure.

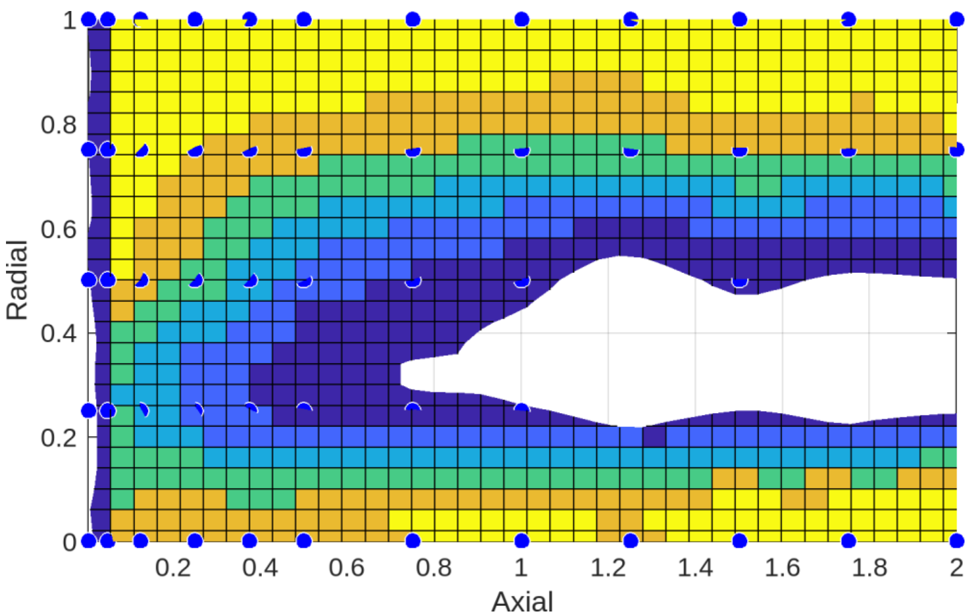

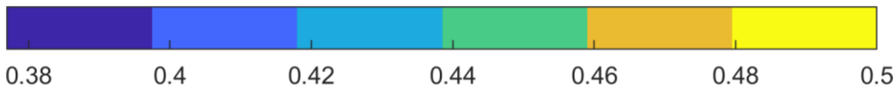

22. Figure. Power coefficients and its regions which are higher than an SRWT's c_p

With the previous figures (Fig. 21 and Fig. 22) we can establish the following:

- The CO-DRWTs in most layouts produce more electricity (based on their overall power coefficient) than a Single Rotor Wind Turbine.
- Between the approx. from R=0.2D and R=0.6D radial distances there is a region where the CO-DRWT's power coefficient is less than an SRTW's.
- Small radial distances (approx. from R=0D to 0.1D) and high radial distances (approx. from R= 0.7D) have a good effect on the CO-DRWT's c_p.

6. Summary

In our paper, we presented an optimisation for a CO-DRWT's (Counter-Rotating Dual Rotor Wind Turbine) spatial arrangement. During our research, we created several layouts for a CO-DRWT which we used within CFD studies. Using the results of the numerical simulation we created surfaces with different interpolation techniques, where we chose a cubic spline interpolation.

For the optimisation method, we used a script for the best and the worst cases. With this script, based on our simulations with our geometry and our boundary conditions, we find the R=0D radial distance with the A=2.1D axial distance has the highest overall power coefficient (c_p=0.514) for the CO-DRWT, while the R=0.35D with A=1.25D distance has the lowest overall power coefficient (c_p=0.354).

By comparison, the c_p of an SRWT (Single Rotor Wind Turbine) which was made with the same geometry and with the same simulation parameters is 0.377. We find some regions where the overall power coefficient of the CO-DRWT is less than the SRWT's, but in most regions, the CO-DRWT's c_p is higher.

Using our results (Fig. 20 and Fig 21) we determined regions where a CO-DRWT has a higher power coefficient than a Single Rotor Wind Turbine. Using this "heat map" we are able to design a small dual-rotor wind turbine which requires less space than two SRWTs have. Therefore in an urbanized region, it could generate more energy than an SRWT, or if it is used in wind farms the farm could have a higher energy density due to the CO-DRWTs' lower space requirement than using traditional wind turbines.

References

[1] F. Szlivka, I. Molnár, "Víz- és szélenergia hasznosítás (Hydro and wind energy utilization)," Edutus Főiskola Kiadó, 2012, https://regi.tankonyvtar.hu/hu/tartalom/tamop412A/2010-0017_10_viz_es_szelenergia/index.html

[2] T. J. Price, "Blyth, James (1839–1906)," *Oxford University Press*, https://doi.org/10.1093/ref:odnb/100957 (Access Date: 08. 09. 2022.)

[3] R. W., Righter, "Wind Energy in America: A History," *University of Oklahoma Press*, ISBN: 9780806128122, 1996., https://books.google.hu/books?id=kGnGw7AEkAEC

[4] *Wind Turbines: the Bigger, the Better*, Office of Energy Efficiency & Renewable Energy (online), https://www.energy.gov/eere/articles/wind-turbines-bigger-better (Access Date: 26. 09. 2022.)

[5] Global Wind Energy Council, 'Global Wind Report 2022," Brussels (Belgium), p. 111., 2022., https://gwec.net/global-wind-report-2022/

[6] Patrick Jackson, *"Ukraine war: EU moves to cut peak electricity use by 5%,"* BBC News (online), https://www.bbc.com/news/world-europe-62899940 (Access Date: 26.09.2022.)

[7] K. R. Kumar, M. Selvaraj, "Review on Energy Enhancement Techniques of Wind Turbine System," *Advances in Science and Technology*, **106**, pp 121-130, 2021., https://doi.org/10.4028/www.scientific.net/AST.106.121

[8] A. Alonso-Estébanez, P. Pascual-Muñoz, F. P. Alvarez Rabanal, D. Castro-Fresno and J. J. Del Coz Díaz, *"New System for the Acceleration of the Airflow in Wind Turbines,"* Recent Patents on Mechanical Engineering, 12(2), pp. 158 - 167., 2019., http://dx.doi.org/10.2174/2212797612666190311154747

[9] M.Anbarsooz, M.Amiri, I.Rashidi, *"A novel curtain design to enhance the aerodynamic performance of Invelox: A steady-RANS numerical simulation"*, Energy, 168, pp. 207-221., 2019., https://doi.org/10.1016/j.energy.2018.11.122

[10] T. Lutz, "Airfoil Design and Optimisation," ZAMM Journal of applied mathematics and mechanics: Zeitschrift für angewandte Mathematik und Mechanik, 81(S3), pp. 787 - 788., 2001., http://dx.doi.org/10.1002/zamm.200108115166

[11] V. M. Kumar, B N. Rao, Sk. Farooq, "Modeling and analysis of wind turbine blade with advanced materials by simulation", International Journal of Applied Engineering Research, 11(6), pp. 4491-4499., 2016., https://www.ripublication.com/ijaer16/ijaerv11n6_128.pdf

[12] W. M. A-Elmagid, I. Keppler, I. Molnár, "Efficient Axial Flow Turbine for Solar Chimney," *Journal of Thermal Science and Engineering Applications*, **12**(3), pp. 031012, 2020., https://doi.org/10.1115/1.4044903

[13] I. Molnár, F. Szlivka, G. Sándor, "Advantages and disadvantages of different types of wind turbines their usage in the city," *WinerCost'17: International Conference on Wind Energy Harvesting*, Coimbra, Portugal, April 20-21, 2017., pp. 269-271, http://www.winercost.com/cost_files/WINERCOST17_Proceedings_Book.pdf

[14] A. Ozbay, W. Tian, H. Hu, "Experimental Investigation on the Wake Characteristics and Aeromechanics of Dual-Rotor Wind Turbines," *Journal of Engineering for Gas Turbines and Power*, **138**(4), pp. 1-15, 2016., https://doi.org/10.1115/1.4031476

[15] E. Erturk, S. Sivrioglu és F. C. Bolat, „Analysis Model of a Small Scale Counter-Rotating Dual Rotor Wind Turbine with Double Rotational Generator Armature," *International Journal of Renewable Energy Research*, **8**(4), pp. 1849-1858, 2018., https://www.ijrer.org/ijrer/index.php/ijrer/article/view/8235

[16] H. Jang, D. Kim, Y. Hwang, I. Paek, S. Kim, J. Baek, "Analysis of Archimedes Spiral Wind Turbine Performance by Simulation and Field Test," Energies, **12**(24), 4624, 2019., https://doi.org/10.3390/en12244624

[17] Nagy A., Jahn I., „Advanced Data Acquisition System for Wind Energy Applications," *Periodica Polytechnica Transportation Engineering*, **47**(2), pp. 124-130, 2019., https://doi.org/10.3311/PPtr.11515

[18] S. Butler, J. Ringwood, F. O'Connor, "Exploiting SCADA system data for wind turbine performance monitoring," 2013 Conference on Control and Fault-Tolerant Systems (SysTol), pp. 389-394, 2013., http://dx.doi.org/10.1109/SysTol.2013.6693951

[19] R. Dziugaite, V. Jankauskas, V. Motuziene, "Energy Balance of a Low Energy House," Journal of Civil Engineering and Management, **18**(3), 2012., pp.369-377., http://dx.doi.org/10.3846/13923730.2012.691107

[20] H. F. Ummah, R. Setiati, Y. B. V. Dadi, M. N. Ariq, M. T. Malinda, "Solar energy as natural resource utilization in urban areas: Solar energy efficiency literature review," IOP Conference Series: Earth and Environmental Science, **780**, 2021., 012007., http://dx.doi.org/10.1088/1755-1315/780/1/012007

[21] Sánta, R. "Comparative Analysis of Heat Pump System with IHX Using R1234yf and R134a," *Periodica Polytechnica Mechanical Engineering*, **65**(4), pp. 363–373, 2021., https://doi.org/10.3311/PPme.18390

[22] A. M. Labib, A. A. Gawad és M. M. Nasseif, „Effect of Aspect Ratio on Aerodynamic Performance of Archimedes Spiral Wind Turbine," EIJEST, 32, pp. 66-72, 2020., https://dx.doi.org/10.21608/eijest.2020.45256.1017

[23] F. Szlivka, I. Molnár, P. Kajtár, G. Telekes, "CFX Simulations by Twin Wind Turbine," *2011 International Conference on Electrical and Control Engineering*, 2011, Yichang, China, 16-18 Sept. 2011. pp. 5780 – 5783, https://doi.org/10.1109/ICECENG.2011.6057550

[24] Cs.Hetyei, F. Szlikva, "Counter-Rotating Dual Rotor Wind Turbine Layout Optimisation", *Acta Polytechnica*, **61**(2), pp. 342–349, 2021., https://doi.org/10.14311/AP.2021.61.0342

[25] A. N. Gorban, A. M. Gorlov, V. M. Silantyev "Limits of the Turbine Efficiency for Free Fluid Flow," *Journal of Energy Resources Technology*, **123**(4), pp. 311-317, 2001., https://doi.org/10.1115/1.1414137

[26] *"List of Library Models for Curve and Surface Fitting,"* MathWorks (online), https://www.mathworks.com/help/curvefit/list-of-library-models-for-curve-and-surface-fitting.html (Access date: 13.07.2022)